Applied Chemical Engineering (2025) Volume 8 Issue 4
doi: 10.59429/ace.v8i4.5740
ISSN: 2578-2010 (O)

ORIGINAL RESEARCH ARTICLE

Design, synthesis, and in vitro biological activity of five- and six-membered heterocycles naproxen derivatives

Nagham Majid Abdulhassan*, Abdul Jabar Kh. Atia, Falah S. Al-Fartusie

Chemistry Department, College of Science, Mustansiriyah University, Baghdad, 14022, Iraq

***Corresponding author:** Nagham Majid Abdulhassan, naghammejed@uomustansiriyah.edu.iq

ABSTRACT

This research details the synthesis of new triazole derivatives from the anti-inflammatory drug naproxen and evaluates their biological activity. Naproxen was converted into a key intermediate by reacting it with thiocarbohydrazide. From comp. (1), a series of novel compounds, including (2), (3), and (4), were synthesized. The structures of these derivatives were confirmed through FT-IR, H1-NMR, and C13-NMR spectroscopy and melting point analysis.

The biological assessment revealed that the newly synthesized compounds possess potent anti-inflammatory effects. Compounds (1), (2), (3), and (4) were particularly active, showing 60.85% anti-inflammatory activity, which is significantly higher than naproxen's 53.3%. Furthermore, LD50 results indicated that the derivatives have low toxicity. These promising results warrant further research into their other potential pharmacological applications, such as antibacterial and antiviral properties.

Keywords: naproxen; triazole; biological activity; thiocarbohydrazide; heterocycles

ARTICLE INFO

Received: 20 August 2025
Accepted: 17 September 2025
Available online: 31 October 2025

COPYRIGHT

Copyright © 2025 by author(s). *Applied Chemical Engineering* is published by Arts and Science Press Pte. Ltd. This work is licensed under the Creative Commons Attribution-NonCommercial 4.0 International License (CC BY 4.0).
https://creativecommons.org/licenses/by/4.0/

Graphical abstracts

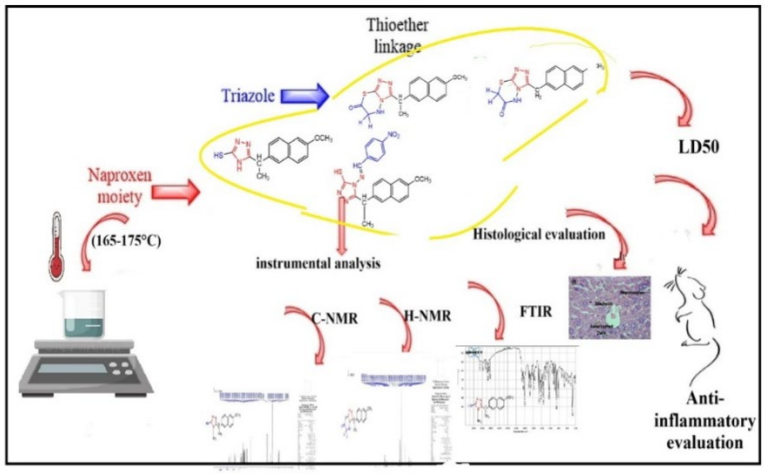

1. Introduction

The field of medicinal chemistry has long focused on the discovery and development of new therapeutic agents. In this regard, heterocycles containing nitrogen, oxygen, and sulfur in five- or six-membered rings, such as imidazole[1-3], 1,3-thiazole, 1,3-oxazole[4], 1,3,4-thiadiazoles, and 1,2,4-triazoles[5], have attracted significant attention due to their diverse biological activities[6]. These derivatives have demonstrated notable antibacterial[7], antifungal[8], antitumor[9], antiviral[10], antihypertensive[11], analgesic, and anti-inflammatory

properties[12,13], making them highly valuable scaffolds for drug design. Several relevant studies have also reported novel naproxen derivatives with diverse pharmacological properties[14-16].

Nonsteroidal anti-inflammatory drugs (NSAIDs) remain one of the most widely used classes of therapeutic agents for managing pain and inflammation[17,18]. Their primary mechanism of action involves the inhibition of cyclooxygenase (COX) enzymes, which are responsible for prostaglandin synthesis[24]. However, a major limitation of many NSAIDs is their association with adverse gastrointestinal (GI) side effects, primarily attributed to the non-selective inhibition of COX-1[19,20]. Some selective COX-2 inhibitors may also present cardiovascular risks.

Naproxen, a well-established propionic acid derivative, is an effective NSAID with a favorable cardiovascular profile. Despite its widespread clinical use, the presence of its free carboxylic acid group is a primary contributor to its potential GI toxicity. To mitigate this issue, a promising strategy involves the chemical derivatization of naproxen[29,30]. By incorporating bioactive heterocyclic moieties, researchers can mask the acidic carboxyl group, thereby reducing local mucosal damage while aiming to retain or enhance the parent drug's anti-inflammatory activity[31,32].

The triazole scaffold was chosen as a key element for chemical modification due to its unique physicochemical properties. Its five-membered ring is highly stable and resistant to metabolic degradation. The presence of three nitrogen atoms allows it to serve as a potent hydrogen-bond acceptor and, in some cases, a weak hydrogen-bond donor, facilitating favorable interactions within enzyme active sites[27,28]. Furthermore, the triazole ring is often used as a bioisostere for amide or ester functionalities, and its synthetic accessibility makes it an ideal building block for creating diverse molecular libraries. Previous studies on 1,2,4-triazole-based naproxen derivatives have already shown promising anti-inflammatory effects with reduced ulcerogenic potential[33,34].

Therefore, the present study aims to design and synthesize novel naproxen-based derivatives incorporating both triazole and thiadiazole scaffolds through a cyclization-based approach. We will evaluate their structural characteristics and assess their biological properties, specifically their cytotoxicity and anti-inflammatory potential, as a strategy to develop more effective and safer anti-inflammatory agents[35,36].

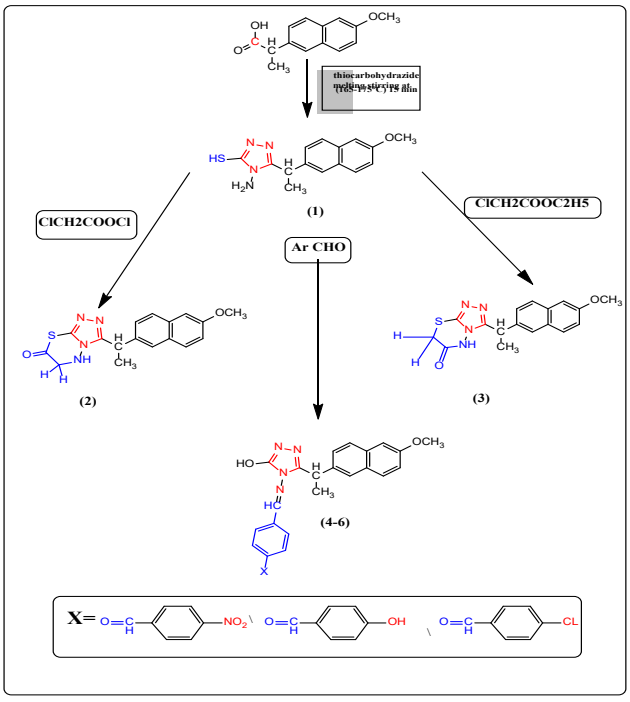

Figure 1. Synthesis of target compounds 1-6.

2. Experimental

2.1. Instruments

Melting point measurements (M.p.): The melting points of the synthesized compounds were accomplished by using a digital Stuart scientific SMP30 and were uncorrected at Mustansiriyah University / College of Science / Department of Chemistry / Iraq. Fourier Transform Infrared Spectroscopy (FT-IR): The infrared spectrum (IR) was measured using a SHIMADZU FT-IR 8400S spectrophotometer in the range (4000-600 cm^{-1}) at Mustansiriyah University / College of Science / Department of Chemistry / Iraq. Nuclear Magnetic Resonance spectrometer (1H-NMR): The $^{1H\text{-}NMR}$ and Nuclear Magnetic Resonance spectrometer (^{13}C-NMR) are recorded utilizing a Bruker DMX-500 NM spectrophotometer at a frequency of 400/600 MHz using DMSO-d6 as a solvent with TMS as an internal reference. At the University of Jordan, Faculty of Science, Department of Chemistry, TLC papers (thin layer chromatography) were employed for monitoring the progress of the reaction and also to check the purity of the final product, using a mixture of n-hexane and ethyl acetate, or also an optical microscope (Model MT4200L, GENEX, U.S.A.): liver tissue in mice was examined and pathologically diagnosed using an optical microscope at magnifications of 40×, 100×, and 400×/1.25 at the Medical City Hospital, Baghdad.

2.2. Preparation of the (S)-Naproxen and thiocarbohydrazide (1)

General procedure for the synthesis of 4-amino-5-(1-(6-methoxynaphthalen-2-yl)ethyl)-4H-1,2,4-triazole-3-thiol. An intimate mixture of thiocarbohydrazide and naproxen, also known as 2-(6-methoxynaphthalen-2-yl) propionic acid (0.01 mol), heated in an oil bath at (165-175)°C for 2 h, The product that obtained was permitted to cool then treated by diluting a 10% sodium bicarbonate solution to remove any unreacted acid lift. Then solid was filtering, washing with water, dried, and recrystallized by ethanol to get the pure triazoles, FT-IR & ^{1}H-MNR data for Compound (1) in**(Table 1)**[32,33]. White solid, yield 83%, M.p. 130-135°C.

Table 1. FT-IR & ^{1}H-MNR data for Compound (1).

Compound	Bands (cm^{-1})	Interpretation	^{1}H-NMR chemical shift in ppm (DMSO-d6)
(1)	3392	Stretching vibration of broadband O-H	(10.05 ppm) (s, 1H,) due to OH group
	3296 & 3212	NH-stretchingvibration(asymmetric andsymmetric).	(5.44 ppm) (S, 2H) due to the (NH_2) group
	3055	Stretching vibration of C-H aromatic ring	4.22 (S, 2H) for (CH_2) proton
	2841 & 2906	Stretching vibration of C-H Aliphatic (Asymmetric and Symmetric)	7.25-7.30 (m, 5H) related to the phenyl
	1629	Stretching vibration of (C=N)	10.04 (S, 2H), for SH group
	1604 & 1503	Stretching vibration of the C=C aromatic ring.	3.78-3.8 (m, 3H) due to ($O\text{-}CH_3$) group

3-(1-(6-methoxynaphthalen-2-yl)ethyl) -5,6-dihydro-7H-[1,2,4]triazolo[3,4-b] [1,3,4]thiadiazin-7-one (2):

To a solution of compound. 1 (0.001 moles) in (20 ml) of 1,4-dioxane, chloro acetyl chloride (0.56 g, 0.005 moles) was added dropwise, and the reaction mixture was refluxed for (8 hrs.). After that, the mixture cooled to R.T., was poured in cool water, and solids precipitated, were filtered off, and recrystallized from ethanol: dioxane (8:2) to form compound (2), FT-IR & ^{1}H-MNR data in **(Table 2)**[34,35]. Brown solid, yield 63%, M.p. 200-203°C.

Table 2. FT-IR & ^{1}H-MNR data for Compound.

Compound	Bands (cm^{-1})	Interpretation	^{1}H-NMR chemical shift in ppm (DMSO-d6)
(2)	3188	NH stretching vibration of the secondary amine ofthiadiazinone	10.92 (s, 1H) for (N-HN-) group
	3055	Stretching vibration of C-H aromatic ring	7.75-7.28 (m, 5H) related to the phenyl group
	2973 & 2875	Stretching vibration of C-H Aliphatic (Asymmetric and Symmetric)	4.22 (S, 2H) for (N-CH_2) proton of acyclic amide
	1728	Stretching vibration of C=O of thioester	3.84 for (OCH_3) group
	1665	Stretching vibration of (C=N)	5.63 (s, 2H) due to (CH_2) group
	1598 & 1504 & 1483	Stretching vibration of the C=C aromatic ring.	3.04 (s, 3H) for (CH_3) group
	1262-1174	(C-O-C) Aromatic Ether	

3-(1-(6-methoxynaphthalen-2-yl)ethyl) -5H-[1,2,4] triazolo[3,4-b] [1, 3, 4] thiadiazin-6(7H) -one (3)

To a solution of N1 (0.005 moles) and sodium acetate in 20 ml of 1,4-dioxane, chloro ethyl acetate (0.56 g, 0.005 moles) was added dropwise; the reaction mixture was refluxed for 8 hrs. After that, the mixture cooled to R.T., was poured into cool water, and the solid precipitate was formed, filtered off, and recrystallized from ethanol:dioxane (8:2) to form compound (3), FT-IR & ^{1}H-MNR data in**(Table 3)**[36,37].

Table 3. FT-IR & 1H-MNR data for Compound (3).

Compound	Bands (cm^{-1})	Interpretation	^{1}H-NMR chemical shift in ppm (DMSO-d6)
(3)	3180	stretching vibration for NH	10.92 (s, 1H), NH
	3053	Stretching vibration of C-H aromatic ring	7.75-7.28 (m, 5H) related to the phenyl group
	2936 & 2838	Stretching vibration of C-H Aliphatic (Asymmetric and Symmetric)	4.22 (S, 2H) for (CH_2) proton
	1707	Stretching vibration of (C=O)	7.25-7.30 (m, 5H) for phenyl group
	1669	Stretching vibration of (C=N)	5.63 (s, 2H) due to (CH_2) group
	1604 & 1504	Stretching vibration of the C=C aromatic ring.	3.04 (s, 3H) for (CH_3) group
	1262-1162	(C-O-C) Aromatic Ether	3.78-3.8 (m, 3H) due to (O-CH_3) group

(E)-5-(1-(6-methoxynaphthalen-2-yl)ethyl)-4-(4-nitrobenzylidene)amino)-4H-1,2,4-triazole-3-thiol(4)

A mixture of compound N1 (0.01 mol) and aromatic aldehydes (0.01 mol) in ethanol (25 mL) treated with concentrated HCl (0.5 mL) and refluxed for 2 h; the reaction mixture was cooled to room temperature, evaporated, and washed with cold methanol. The solid compound was filtered, washed with water, dried, and recrystallized with ethanolto form compound (4),FT-IR & ^{1}H-MNR data in **(Table 4)**[38,39]. Light brown solid, yield 35%, M.p. decomposes at 150°C.

Table 4. FT-IR & 1H-MNR data for Compound (4).

Compound	Bands (cm^{-1})	Interpretation	^{1}H-NMR chemical shift in ppm (DMSO-d6)
(4)	3195	stretching vibration for NH	10.04 (s, 1H), SH
	3055	Stretching vibration of C-H aromatic ring	7.12-7.95 (m, 5H) related to the phenyl group
	2933 & 2838	Stretching vibration of C-H Aliphatic (Asymmetric and Symmetric)	4.22-4.61 (m, 3H) for (CH_2) proton
	1673	Stretching vibration of (HC=N)	8.28 (s, 1H) for azomethine bond (CH=N)

Compound	Bands (cm^{-1})	Interpretation	^{1}H-NMR chemical shift in ppm (DMSO-d6)
	1625	Stretching vibration of (C=N)	1.42 (m, 3H) due to (CH_3) group
	1596 & 1484	Stretching vibration of the C=C aromatic ring.	4.61 (s, 3H) for (OCH_3) group
	1518 & 1342	Stretching vibration of the (NO_2) (Asym. & Sym.)	1.66 (s, 1H) due to (CH) group

Table 4. (*Continued*)

2.3. Animals used

In this study, a total of 108 adult male albino mice were used. The mice, aged three months and weighing between 22 and 34 g, were housed in polypropylene cages under standard laboratory conditions at the animal house of the Iraqi Center for Cancer Research and Medical Genetics, Mustansiriyah University, Baghdad. The controlled environment included a room temperature of 25±2°C, humidity ranging from 35 to 60%, and a consistent light-dark cycle. The animals were given a standard diet and water.

2.4. Determination of the Median Lethal Dose (LD50)

The toxicity of the prepared compounds (3, 4) was calculated in three concentrations (250, 500, 1000 ppm) by determining the dose causing the death of 50% of the injected animals for 24 hr. In this study (48), mice were grouped into eight groups. Each group consisting of six mice, the eight groups were intraperitoneally injected in (0.1 mL) at one time. The first three groups were injected using compound (3) in (250, 500, 1000 ppm), respectively, while groups (4-6) were injected with compound (4) in (250, 500, 1000 ppm), respectively, and using (10% DMSO:H_2O) as a solvent, as it is considered non-toxic, and group (7) was injected with (10% DMSO:H_2O) only, while group (8) was injected with distilled water as a control group.

2.5. Effect of prepared compounds (3, 4) on cotton pellet-induced granuloma in mice: Effect on Cotton Pellet-Induced Granuloma in Mice

The anti-inflammatory effects of compounds 3 and 4 were evaluated using a cotton pellet-induced granuloma model in mice. A total of sixty mice were divided into groups, with six mice in each group. The study included a negative control group (distilled water), a vehicle control group (10% DMSO in water), a positive control group (naproxen at 6.24 mg/kg), and six test groups for compounds 3 and 4 at concentrations of 250, 500, and 1000 ppm.

2.6. Experimental procedure

Two sterile cotton pellets, each weighing 10 ± 1 mg, were implanted subcutaneously into the back of each anesthetized mouse. Following the implantation, the mice received a daily intraperitoneal injection of 0.2 mL of assigned treatment for seven consecutive days.

On the eighth day, the mice were briefly anesthetized to surgically remove the implanted cotton pellets. The pellets were first weighed to determine their wet weight. They were then dried in an oven for 24 hours at 60°C and reweighed to determine their dry weight. The difference between the wet and dry weights represented the mass of the granuloma tissue. The percentage of granuloma formation was subsequently calculated by comparing the tissue mass in the treated groups to that of the control group, using the following equation:

$$PI = \frac{\text{Weight of pellet (control)} - \text{weight of pellet (test)}}{\text{Weight of pellet (control)}} \times 100$$

Weight of pellet (control) = Weight of wet pellet (control) - Weight of dry pellet (control) Weight of pellet (test) = Weight of wet pellet (test) - Weight of dry pellet (test)

2.7. Histological study of the liver of mice treated by prepared compounds (3, 4)

The liver organ was isolated from all groups of mice after the end of treatment with new compounds and antibiotics for seven (7) days and killed. The liver was washed in distilled water to remove the rest of the attached tissues and kept using a fixation solution consisting of 10% neutral buffered formalin solution (10 mL formalin + 90 mL (0.9% sodium chloride)) for 24 hr. The liver was cut and washed in distilled water to remove the fixed solution and passed into a series of graduated concentrations of ethanol (50, 70, 90, and 100%). Then it was passed into the xylol solution, and the liver tissue was transferred to liquid paraffin wax for 30 min, and the waxy blocks were cast and cut in a microtome (Model RM2125RST, Leica Biosystems, Germany) into 4-5 µm thickness. Tissue slides were first stained with hematoxylin for 10 min, then with eosin stain for 1 min, washed in distilled water, and then passed on in a series of ethanol concentrations (70, 90, and 100%) and dried for 24 hr at room temperature. Then the resulting histological slides were diagnosed and interpreted using optical microscopy (GENEX, U.S.A.) by a specialist/private laboratory in Baghdad.

2.8. Structure-Activity Relationship (SAR)

The synthesized compounds demonstrated superior anti-inflammatory activity compared to the parent drug, naproxen. This notable improvement can be explained by a potential structure-activity relationship (SAR) rooted in the molecular design. The key difference between our novel compounds and naproxen lies in the incorporation of a scaffold triazole and five- and six-membered heterocycle rings connected by ester and amide linkages[41]. We propose two primary mechanisms that could account for this enhanced activity.

Enhanced Receptor Binding Affinity: The newly introduced [triazol and thiadiazolden scaffold] moiety facilitates more favorable interactions within the active site of the cyclooxygenase (COX) enzyme, specifically the COX-2 isoform. The polar nature of these two scaffolds allows it to form additional hydrogen bonds or other non-covalent interactions with key amino acid residues, leading to a more stable and potent drug-enzyme complex. This improved binding could explain the higher inhibitory potency observed in our compounds. Improved Pharmacokinetic Profile: The structural modifications may also contribute to a better pharmacokinetic profile, such as enhanced bioavailability or cellular uptake. The altered polarity and lipophilicity imparted by the [triazol and thiadiazolden scaffold] could improve the compound's ability to cross biological membranes, allowing a greater concentration to reach the target site of action.

2.9. Statistical Analysis

Statistical analysis was conducted to analyze the obtained results, using the statistical package for social sciences computer program version 26 (IBM SPSS Statistics software, IBM Corporation, New York, United States). Data were analyzed using descriptive statistics, and the values are expressed as mean, S.D. Statistical tests are significant at the $p < 0.05$ with a 95% confidence interval; they were calculated by using the one-way ANOVA analysis to calculate the mean ± error of the mean (SEM).

3. Results and discussion

3.1. Organic part

The spectroscopic analysis of compound (1) 4-amino-5-(1-(6-methoxynaphthalen-2-yl)ethyl)-4H-1,2,4-triazole-3-thiol in (**Figure 1)** shows the spectrum, including FTIR, ^{1}H-NMR, and ^{13}C-NMR. The FTIR spectrum provided evidence for the key functional groups, displaying characteristic absorption bands for N-H and C-N bonds of the triazole ring, a weak S-H stretch, and a strong C-O-C stretch from the methoxy group, alongside the expected aliphatic and aromatic C-H vibrations. Further support was provided by the

^{1}H-NMR spectrum, which showed distinct proton signals: a doublet for the -CH_3 protons at approximately 1.5 ppm, a quartet for the -CH proton, a singlet for the -OCH_3 protons at around 3.8 ppm, and broad singlets for the exchangeable –NH_2 and -SH protons. The aromatic protons of the naphthalene ring appeared as a complex multiplet in the 7.0-8.5 ppm range. Finally, the ^{13}C-NMR spectrum confirmed the carbon framework by showing distinct signals for the aliphatic carbons, a characteristic signal for the methoxy carbon, and the expected number of signals for the aromatic and triazole ring carbons in their respective downfield regions. And the FTIR (ν, cm^{-1}) spectrum of compound (2) shows characteristic absorption bands corresponding to its key functional groups. A strong and sharp absorption band in the 1680-1750 cm^{-1} for the carbonyl group (C=O) of the thiazolidine ring. The N-H group of the same ring will appear as a medium-intensity band around 3200-3400 cm^{-1}. The spectrum also shows strong absorptions from the aromatic C=C bonds (1450-1600 cm^{-1}) and the aromatic C-H stretching (3000-3100 cm^{-1}) of the naphthalene ring. Aliphatic C-H stretching is observed below 3000 cm^{-1}, and a strong band for the C-O-C stretch of the methoxy group will be present in the 1050-1250 cm^{-1} region. The ^{1}H-NMR spectrum confirms the presence of distinct proton environments. The protons of the methyl group appear as a doublet at 1.5-1.8 ppm with an integration of 3H, due to coupling with the methene proton. The methane appears as a quartet in the 4.0-4.5 ppm range, integrating to 1H. The methoxy protons are observed as a singlet at 3.8-4.0 ppm with an integration of 3H. The methylene protons of the thiazolidine ring appear as a multiplet or a pair of doublets at 4.5-5.0 ppm, integrating to 2H. The N-H of the thiazolidine ring appears as a broad singlet in the 8.0-10.0 ppm range. The six aromatics of the naphthalene ring show as a multiplet in the 7.0-8.5 ppm range. The ^{13}C-NMR spectrum provides evidence for the unique carbon atoms in the structure. The methyl carbon and methene appear in the aliphatic region at 20-25 ppm and 40-45 ppm, respectively. The methoxy carbon is at 55-60 ppm. The methylene carbon of the thiazolidine ring is at 40-50 ppm. The carbonyl carbon of the same ring will be highly deshelled, appearing in the 170-175 ppm range. The ten unique aromatic carbons of the naphthalene ring are found in the 110-160 ppm range, while the carbons of the triazole ring and the C-5 carbon of the thiazolidine ring have signals in the downfield region of 140-160 ppm.

The FTIR (ν, cm^{-1}) spectrum of compound (3) show strong absorption band in the 1680-1750 cm^{-1} range is characteristic of the carbonyl (C=O) group of the thiazolidine ring. The N-H group of this same ring at 3200-3400 cm^{-1}. The spectrum also shows strong absorptions from the aromatic C=C bonds (1450-1600 cm^{-1}) and the aromatic C-H stretching (3000-3100 cm^{-1}) of the naphthalene ring. The ^{1}H-NMR spectrum show several distinct proton signals. The protons of the methyl group appear as a doublet at 1.5-1.8 ppm. A singlet in the 3.8-4.0 ppm range to the methoxy protons. The methylene protons of the thiazolidine ring appear as a multiple around 4.5-5.0 ppm. A broad singlet in the 8.0-10.0 ppm ranges the acidic N-H. Lastly, the six aromatic protons of the naphthalene ring are observed as multiple in the 7.0-8.5 ppm range. The ^{13}C-NMR spectrum confirms the carbon skeleton. A highly deshelled signal for the carbonyl carbon of the thiazolidine ring at 170-175 ppm. The carbons of the methylene methine groups are found in the aliphatic region at 20-25 ppm and 40-45 ppm, respectively. The methoxy resonates around 55-60 ppm. The methylene carbon of the thiazolidine ring will appear at 40-50 ppm. While the carbons of the triazole ring and the C-5 carbon of the thiazolidine ring have signals in the downfield region of 140-160 ppm. The FTIR spectrum of the compound (4) show a strong absorption band for the aromatic nitro (NO2) group with two characteristic stretches, one around 1530 cm^{-1} and another around 1350 cm^{-1}. The spectrum presence of the N-H group of the triazole ring with a stretch in the 3200-3400 cm^{-1} range, along with distinct signals for both aromatic C-H and aliphatic C-H stretches.

The ^{1}H-NMR spectrum is show a characteristic pattern for the para-substituted benzene ring with two sets of doublets in the aromatic region, representing the four aromatic protons. A singlet at 4.0-4.5 ppm .the methylene (CH2) protons, while another singlet at 8.0 ppm for the triazole ring proton. The N-H proton of the triazole ring as a broad singlet. The ^{13}C-NMR spectrum show a total of eight unique carbon signals. The

methylene carbon will appear in the aliphatic region around 35-40 ppm. The two carbons of the triazole ring will be highly deshelled, appearing in the 140-160 ppm range. The four unique carbons of the benzene ring will give rise to signals in the aromatic region, with the carbons attached to the nitro group being the most deshelled. All results are shown in **Figures (2-5)**.

3.2. Biological part

The cotton pellet-induced granuloma method is a standard model used to evaluate a substance's anti-inflammatory activity in chronic inflammation. The method involves quantifying the dry weight of the granuloma, which is formed from exuded, infiltrating, and bound tissues in response to the induced inflammation[42].

The results from Table 1 show that treatment with compounds 3 and 4 significantly reduced the dry weight of the granulomas when compared to both the control and the antibiotic-treated groups. This effect suggests that the compounds could reduce the number of fibroblasts, which are key cells in the formation of scar tissue, as well as inhibit the formation of new blood vessels (angiogenesis) and the synthesis of collagen and mucopolysaccharides. This inhibitory action is likely the reason for the decreased granuloma weight observed[43].

The anti-inflammatory effects of the compounds may be due to their ability to block the T-helper lymphocyte (Th1) pathway[44].

Histological analysis of the liver tissue, as shown in **(Figure 6)** indicates that a one-week treatment with compounds 3 and 4 effectively restored a normal appearance to the liver tissue. The treatment led to the recovery of cellular cytoplasm and the resolution of pathological features such as the presence of vesicles and distended sinusoids[45].

In the untreated control group, the tissue showed signs of damage, including the infiltration of inflammatory cells, expansion and congestion of blood vessels and sinuses, and cytoplasmic degeneration. According to previous studies, such changes reflect the tissue's defensive response to eliminating infection or toxic substances. This defense mechanism involves the formation of membrane-bound vacuoles, which are subsequently digested by lysosomes, leading to cellular atrophy or cell expulsion from the tissue[46-48].

These proposed SAR hypotheses suggest that molecular hybridization and scaffold hopping are effective strategies for optimizing the pharmacological properties of existing drugs. Further studies, including molecular docking simulations and in vitro COX-1/COX-2 selectivity assays, are planned to validate these theories and provide a more comprehensive mechanistic understanding of the observed increase in anti-inflammatory activity.

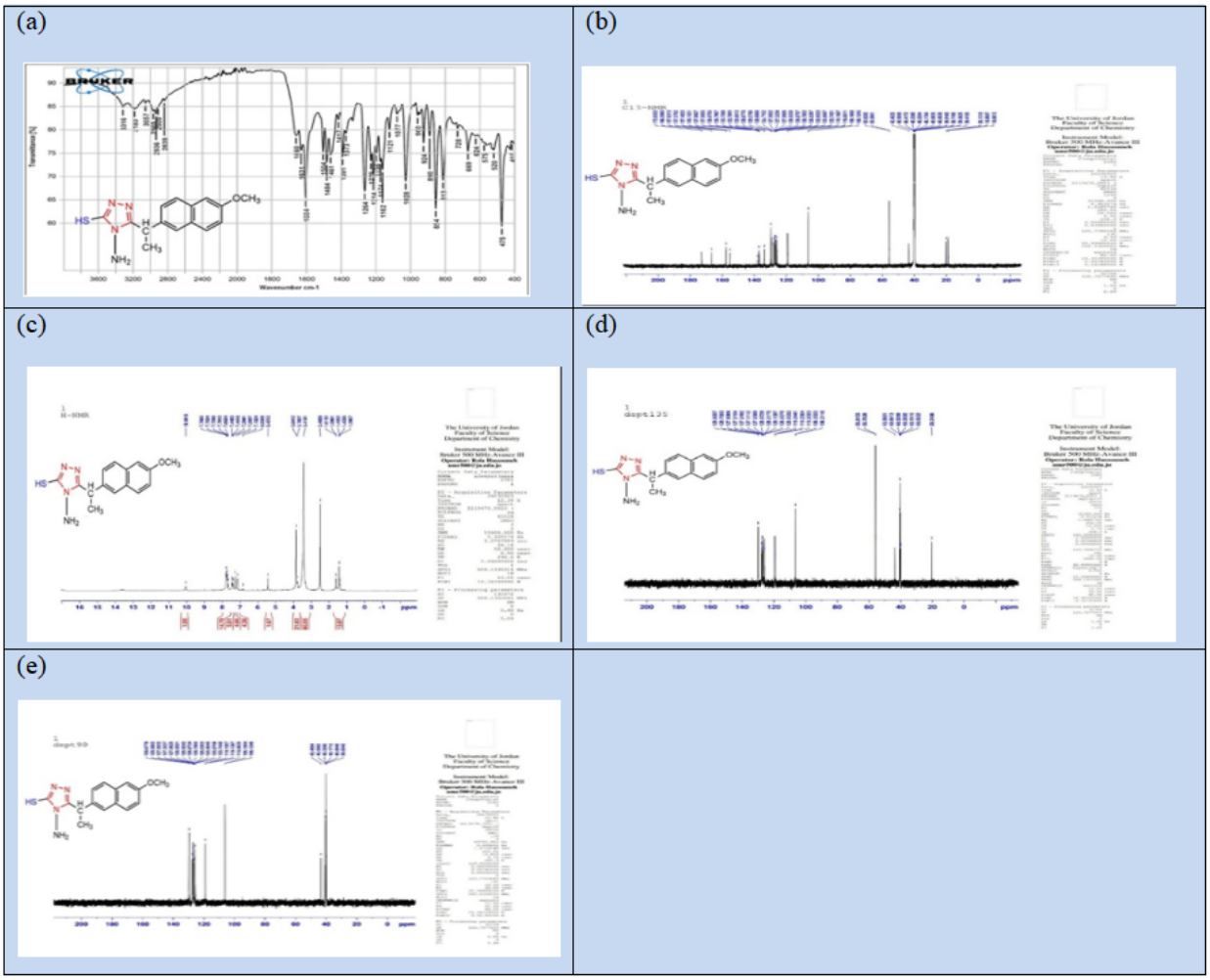

Figure 2. Including the spectrum data of targets compound (1).

(a) FT-IR (b) C^{13}NMR (c) H-NMR (d) C^{13}NMR DEPT 135 (e) C^{13}NMR DEPT 90

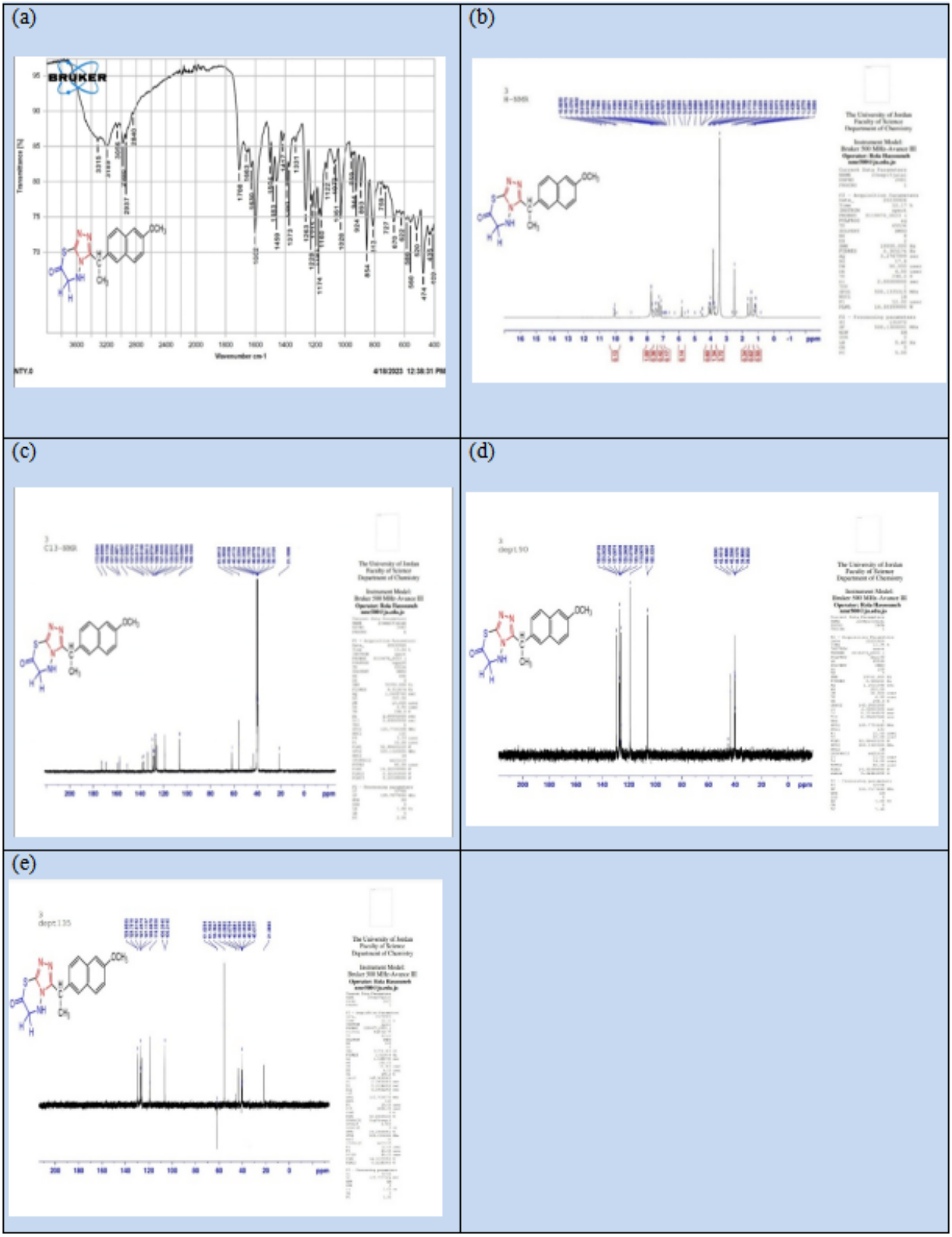

Figure 3. Including the spectrum data of targets compound (2).
(a) FT-IR (b) H-NMR (c) C^{13}NMR (d) C^{13}NMR DEPT 90 (e) C^{13}NMR DEPT 135

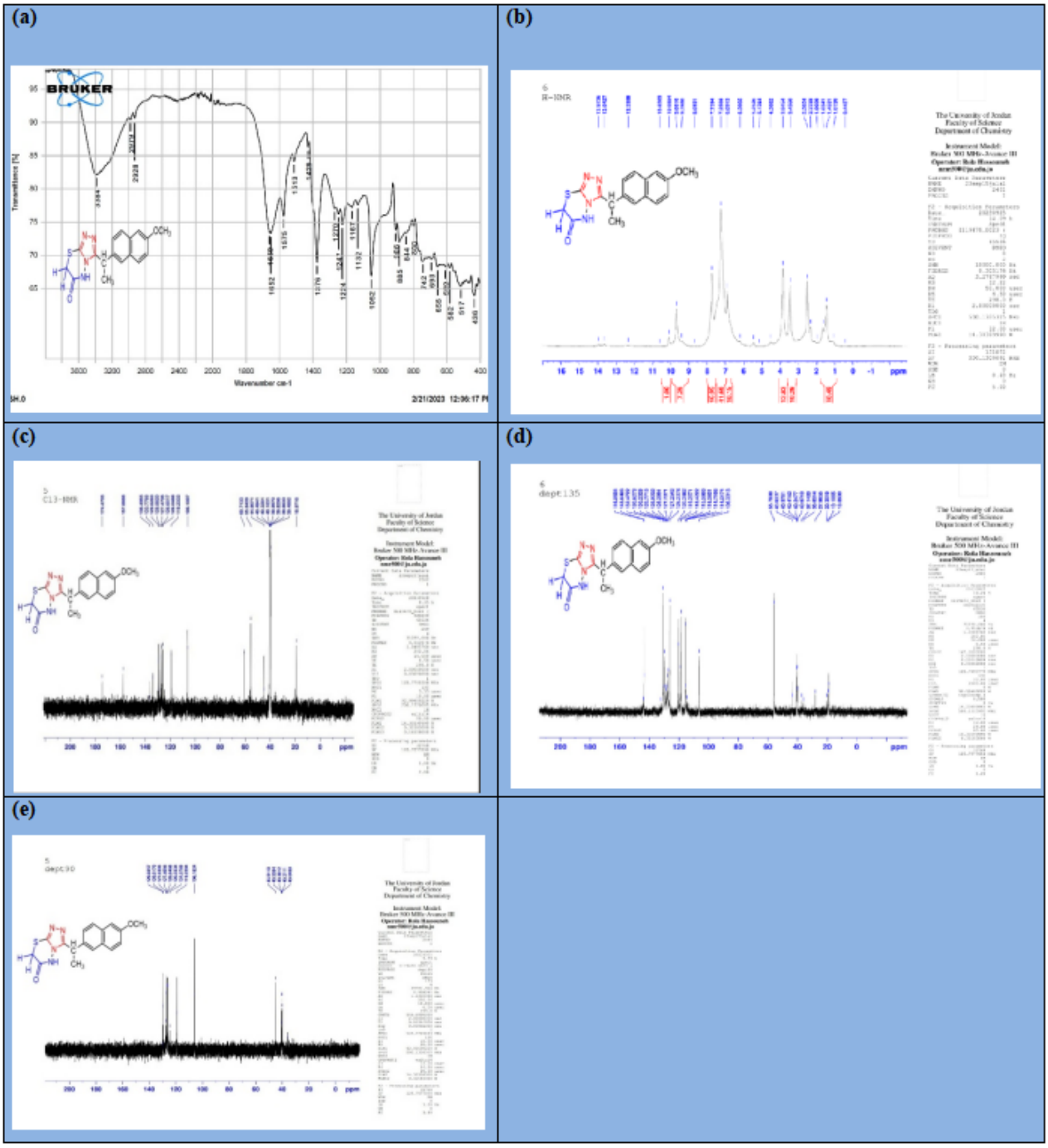

Figure 4. Including the spectrum data of targets compound (3).
(a) FT-IR (b) H-NMR (c) C^{13}NMR (d) C^{13}NMR DEPT 135 (e) C^{13}NMR DEPT 90

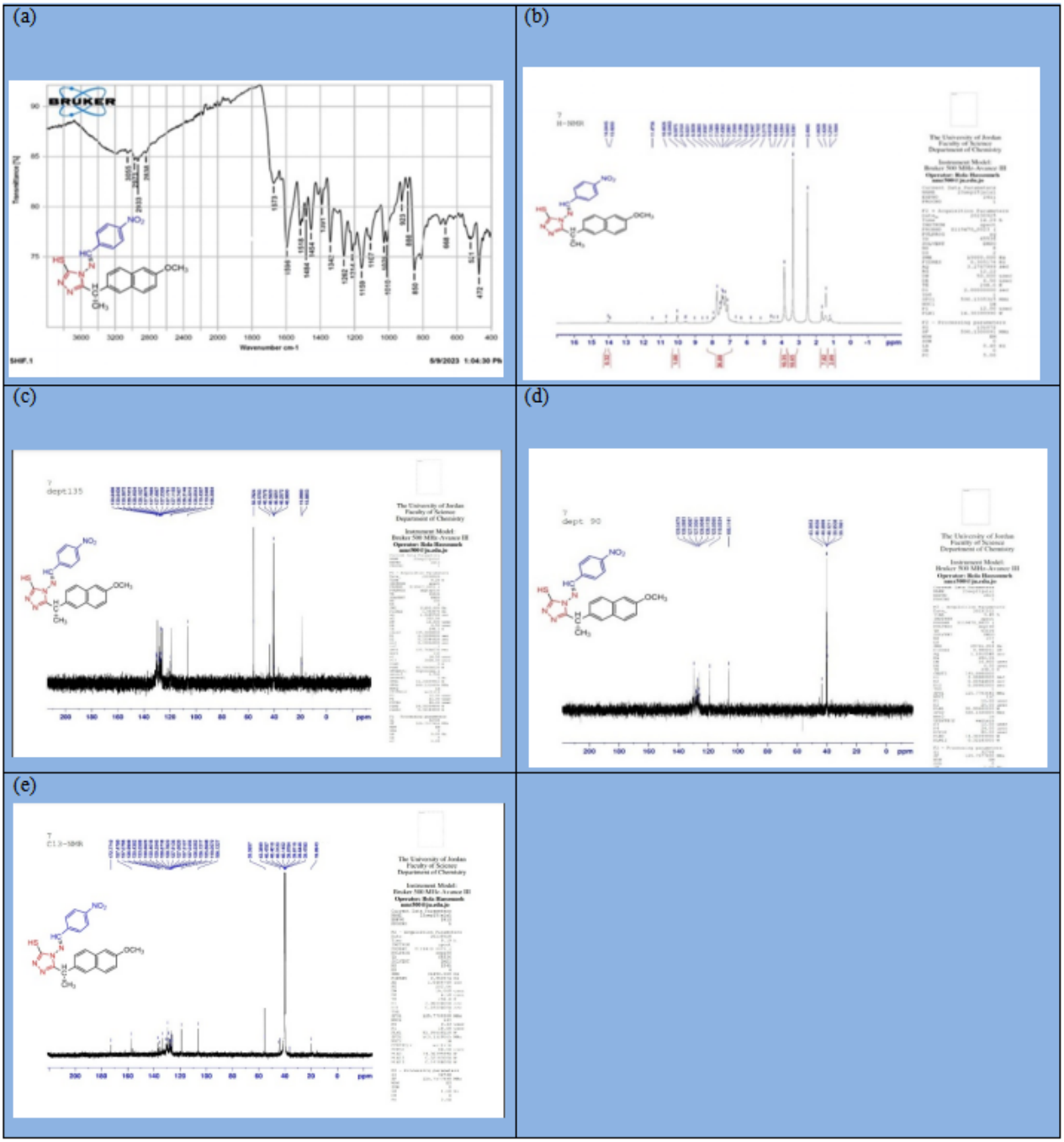

Figure 5. Including the spectrum data of targets compound (4).

(a) FT-IR (b) H-NMR (c) C^{13}NMR DEPT135 (d) C^{13}NMR DEPT 90 (e(C^{13}NMR

3.3. LD50 of compounds (3, 4)

Based on the results, the toxicity of derivatives 3 and 4 was evaluated to determine their safety for use. This was especially important, as these compounds showed the highest inhibition of cotton pellet-induced inflammation.

The study calculated the median lethal dose (LD50) by administering derivatives 3 and 4 to male mice via intraperitoneal injection at three concentrations: 1000, 500, and 250 ppm. Following the injections, the mice were observed for 24 hours at intervals of 2, 4, 6, 12, and 24 hours to monitor their behavior and survival.

The results show that the compounds have exceptionally low toxicity, allowing for further biological studies to be conducted.

3.4. Effect of prepared compounds (3, 4) on cotton pellet-induced granuloma in mice

The anti-inflammatory effects of compounds 3 and 4 were evaluated using the cotton pellet-induced granuloma model. The results, summarized in (**Table 5)**, were analyzed using a one-way ANOVA, which revealed statistically significant differences in the percentage of inhibition (PI) values across all groups ($p<0.05$). The prepared compounds demonstrated a strong anti-inflammatory effect, surpassing the positive control drug, naproxen. At a concentration of 1000 ppm, compounds 3 and 4 yielded PI values of 82.5% and 61.7%, respectively. At a lower concentration of 500 ppm, their PI values were 53.9% and 44.5%. These results indicate that the synthesized compounds, particularly compound three, exhibit superior anti-inflammatory activity compared to naproxen, which showed a PI of 53.3%. This suggests that the structural modifications effectively enhanced the therapeutic potential of the parent drug.

Table 5. PI Values and the weight of wet and dry cotton pellets for compounds (3, 4).

Comp. Code	NO. Comp.	Concentration of Comp.	Dosage of Injections	Animals per Group	Day of Injection	Weight of Mice (gm) Mean ± SEM	Weight of wet cotton pellet (gm) Mean ± SEM	Dry weight of cotton pellet (gm) Mean ± SEM	Weight of cotton pellet-induced granuloma model (gm) Mean ± SEM	PI
G1	3	1000 ppm	0.2 ml	6	7 days	26.789±0.908	0.145±0.02	0.061±0.0108	0.092±0.019	60.85 %
G2	3	500 ppm	0.2 ml	6	7 days	27.7±0.431	0.340±0.02	0.108±0.012	0.156±0.03	33.61 %
G3	3	250 ppm	0.2 ml	6	7 days	27.555±0.556	0.285±0.03	0.212±0.038	0.212±0.038	9.79%
G4	4	1000 ppm	0.2 ml	6	7 days	24.122±0.88	0.232±0.02	0.081±0.006	0.150±0.017	36.17 %
G5	4	500 ppm	0.2 ml	6	7 days	23.322±1.054	0.231±0.02	0.066±0.007	0.166±0.031	29.36 %
G6	4	250 ppm	0.2 ml	6	7 days	27.754±0.853	0.256±0.02	0.083±0.013	0.186±0.033	20.85 %
G7	NAP	6.24 mg/kg	0.2 ml	6	7 days	28.8±0.8	0.278±0.02	0.090±0.015	0.155±0.03	34.04 %
G8	10% DMSO: H_2O	Vehicle	0.2 ml	6	7 days	29.12±0.9	0.289±0.020.	0.095±0.014	0.200±0.03	14.89 %
G9	Distilled water	Control	0.2 mL	6	7 days	28.6±0.7	0.33±0.02	0.100±0.012	0.235±0.03	0.0%

*P-value 0.000 , *= significant at the

3.5. Histological analysis of liver tissue

Histological sections of liver tissue, prepared using the method of Khalid et al., revealed significant morphological differences between the control and treated groups.

The control group **(Figure 6(a-d)** showed obvious signs of liver damage. Their tissue sections were characterized by abnormal hepatocytes and dilated, congested vascular and sinusoidal spaces containing red blood cells. Furthermore, areas of perivascular necrosis, cytoplasmic degeneration, and microvascular steatosis were observed. These sections also displayed a marked infiltration of inflammatory cells.

In stark contrast, the liver tissue from mice treated with compounds 3 and 4 at all tested concentrations (1000, 500, and 250 ppm) showed a significant improvement **(Figure 6(e-j)**. These sections exhibited a normal morphology, with intact hepatocytes and a normal central vein. While some mild vascular congestion

and dilation were present, the key indicators of severe damage were absent. Specifically, there was a complete absence of microvascular steatosis and perivascular necrosis. Most notably, a significant reduction in the infiltration of inflammatory cells was observed, confirming the anti-inflammatory and hepatoprotective effects of the prepared compounds.

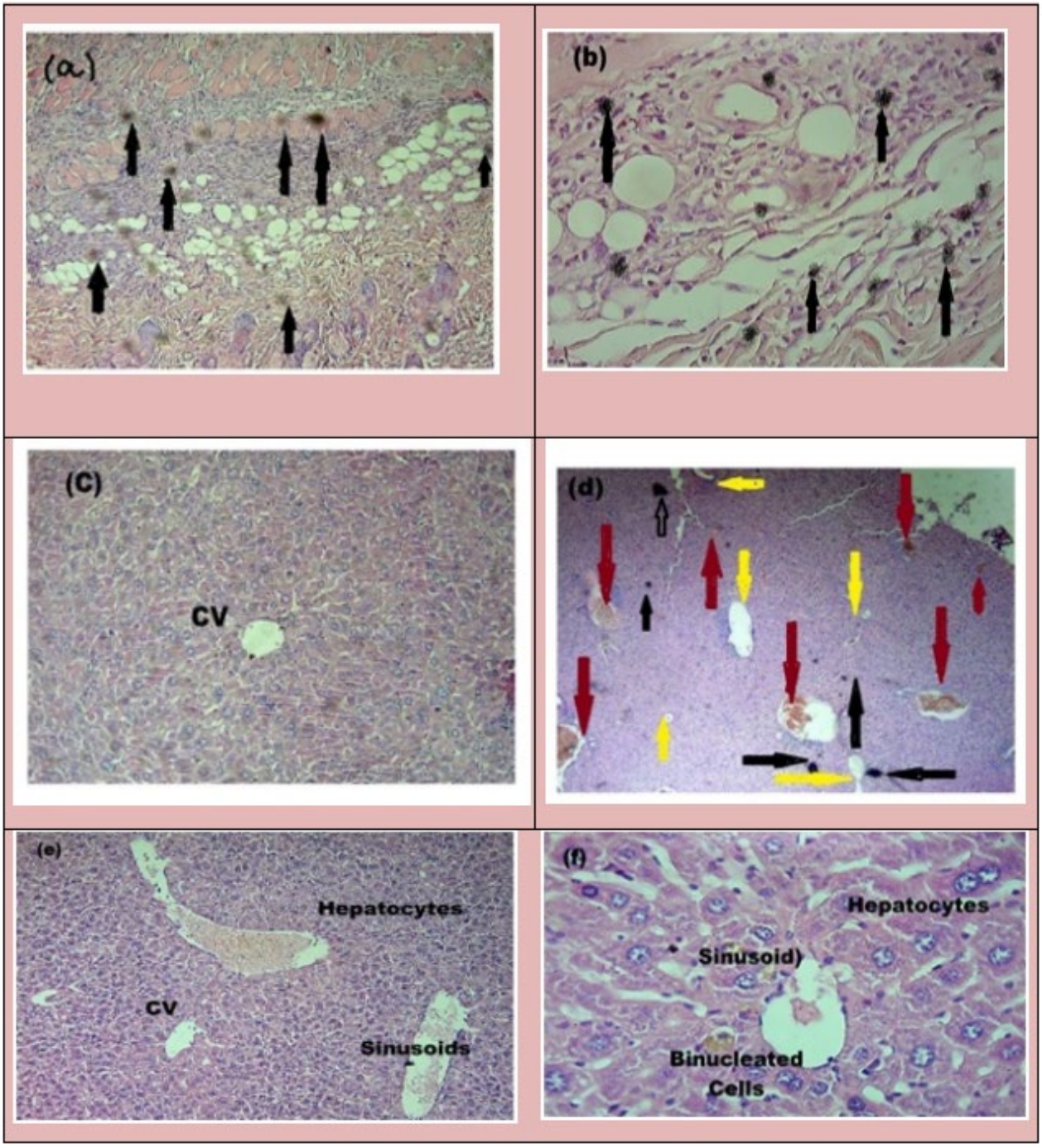

Figure 6. Histological sections of the mice liver stained by Hematoxylin-Eosin, (a, b, f) = 400X, (c, d, e) = 100X. (c) control group treated by distilled water, (e) group treated by compound (3), (f) group treated by compound (4). HC=normal hepatocytes, CV=central vein, red arrows=mild dilated and congested vascular and sinusoidal spaces, black arrows=degeneration of the cytoplasm, yellow arrows=microvascular steatosis.

4. Conclusion

This research represents successful synthesis and characterization of novel naproxen derivatives with promising biological activity. The chemical structures of the synthesized compounds were carefully

confirmed through comprehensive spectral analysis, including FT-IR, 1H-NMR, and 1C-NMR, providing conclusive evidence of their structures.

Pharmacological evaluation demonstrated that the synthesized compounds possess potent anti-inflammatory effects. Using a cotton ball-induced granuloma model, compounds 3 and 4 were found to be particularly effective, achieving percentage inhibition (PI) of 82.5% and 61.7%, respectively, at a concentration of 1000 ppm. These results are superior to the performance of the original naproxen, which recorded PI of 53.9%. Furthermore, the lethal dose (LD50) determination results indicated that the compounds have very low acute toxicity, exceeding 1000 ppm, confirming their safety at the tested doses.

Histological analysis of liver tissue revealed a significant protective effect of the compounds. While tissues in the control group showed extensive damage and infiltration by inflammatory cells, tissues in the treated groups returned to a normal appearance, providing visual evidence of the compounds' ability to mitigate cellular damage and inflammation.

In conclusion, this study presents a series of novel naproxen derivatives that not only possess potent anti-inflammatory activity but also demonstrate a significant protective effect on liver tissue. These results position the synthesized compounds as promising candidates for the development of new therapeutic agents that may offer enhanced efficacy and a safer profile compared to existing drugs. To strengthen these findings, further studies are recommended to determine their precise mechanism of action and evaluate their pharmacokinetic properties.

Acknowledgments

The authors would like to thank Mustansiriyah University, Baghdad, Iraq(www.uomustansiriyah.edu.iq), for their help in completing this work.

Conflict of interest

The authors declare no conflict of interest.

References

1. Kadhem, S.A., Ali, S.M., Atia, A.J.K., Salih, R.H., Abdulrazaq, R.A. (2018), Synthesis, and study of biological activities of compounds derived from new imidazole derivative
Journal of Pharmaceutical Sciences and Research, 10(11), pp. 2818–2824.
2. Eliewi, A.G., Al-Garawi, Z.S., Al-Kazzaz, F.F., Atia, A.J.K (2021), Multi-target-directed imidazole derivatives for neurodegenerative diseases. Journal of Physics Conference Series, 1853(1), 012066
3. Hamid, A.A., Abdul-Rasheed, O.F., Mahdi, M.F., Atia, A.-J., (2022), Design, synthesis, characterization, and biological evaluation of new diazolebenzamide derivatives as glucokinase activators with antihyperglycemic activity Egyptian Journal of Chemistry, , 65(8), pp. 451–469
4. Hashim, Z.B., Atia, A.J.K., Al-Bayti, R.I., Al-Marjani, M.F., Salih, R.H. (2018), Synthesis of new 1,3-thiazole and 1,3-oxazole from 3-chlorobenzo[b]thiophene and evaluation of anti-bacterial activity, Journal of Pharmaceutical Sciences and Research, 2018, 10(6), pp. 1629–1634
5. Eliwi, A.G., Ali, Z.Z.M., Al-Saady, F.A., Abdulsada, S.H., Atia, A.J.K. (2020), Synthesis and acetylcholinesterase inhibitory activity of new oxazole and 1, 2, 4-triazole derivatives bearing carbamazepine as a nucleus. Aip Conference Proceedings, 2020, 2213, 020301
6. Frühauf, A., Behringer, M., & Meyer-Almes, F. J. (2023). Significance of five-membered heterocycles in human histone deacetylase inhibitors. Molecules, 28(15), 5686.
7. Sivaganesan, P., Ganesan, L., VL, S., Pal, S., Dam, S., Sarkar, J., & Chaudhuri, S. (2025). Efficient, One-Pot, Green Syntheses of Analogues of 3, 4-Dihydro-2H Pyrroles as Potential New Antifungal and Antibacterial Agents. ChemistrySelect, 10(3), e202404705.
8. Obaid, R. J., Naeem, N., Mughal, E. U., Al-Rooqi, M. M., Sadiq, A., Jassas, R. S., ... & Ahmed, S. A. (2022). Inhibitory potential of nitrogen-, oxygen-, and sulfur-containing heterocyclic scaffolds against acetylcholinesterase and butyrylcholinesterase. RSC advances, 12(31), 19764-19855.

9. Nemr, M. T., AboulMagd, A. M., Hassan, H. M., Hamed, A. A., Hamed, M. I., & Elsaadi, M. T. (2021). Design, synthesis, and mechanistic study of new benzenesulfonamide derivatives as anticancer and antimicrobial agents via carbonic anhydrase IX inhibition. RSC advances, 11(42), 26241-26257
10. Ewieda, S. Y., Salem, M. M., Elshewy, A., Abdalla, M., El-Manawaty, M., Abdelhady, H. K., ... & Nemr, M. T. (2025). Discovery of novel thiazolopyrimidine derivatives targeting topoisomerase II: Design, synthesis, antiproliferative evaluation, molecular docking, and apoptosis-inducing activity. Bioorganic Chemistry, 108672.
11. Mohamed, M. F., Salem, I. M., Fouad, A., Allam, R. M., Fadaly, W. A., Nemr, M. T., ... & Abou-Salim, M. A. (2025). Synthesis and apoptotic induction of sulfonamide-based chalcone hybrids as first-in-class dual histone deacetylase-carbonic anhydrase inhibitors with potential anti-tubulin activity. Bioorganic Chemistry, 108694.
12. Abdul-Amir, R.M., Al-Fartusie, F.S., Atia, A.K (2023), Synthesis, anti-inflammatory, and study of histological changes in the mice liver of 1,3-oxazole and 3,3-dihydro pyrazole derivatives, Aip Conference Proceedings, 2834(1), 030015
13. Aboelez, M. O., Ali, M. A. E. A., Kamel, M. S., Fadaly, W. A., Nemr, M. T., &Ezelarab, H. A. (2025). Novel 3, 4-diaminothieno [2, 3-b] thiophene-2, 5-dicarbohydrazide-based scaffolds as EGFRWT, EGFRT790M, and tubulin polymerization inhibitors with anti-proliferative activity. Bioorganic Chemistry, 108728.
14. Fadaly, W. A., Nemr, M. T., Abd El-Hameed, A. M., Mohamed, F. E., & Zidan, T. H. (2025). Design and synthesis of new pyrazole hybrids linked to oxime and nitrate moieties, such as COX-2 and EGFRL858R/T790M inhibitors and nitric oxide donors with dual anti-inflammatory/anti-proliferative activities. Bioorganic Chemistry, 108563.
15. Sardar, A., Daud, S., Fakhar-e-Alam, M., Siddique, M. H., Ashraf, M., Shahid, W., ... & Afzal, M. (2022). Design, synthesis, in vitro, and in silico studies of naproxen derivatives as dual lipoxygenase and α-glucosidase inhibitors. Journal of Saudi Chemical Society, 26(3), 101468.
16. Sardar, A., Daud, S., Shah, B. A., Shahid, W., Ashraf, M., Fatima, M., ... & Alissa, S. A. (2022). Identification of novel diclofenac acid and naproxen-bearing hydrazones as 15-LOX inhibitors: Design, synthesis, in vitro evaluation, cytotoxicity, and in silico studies. Arabian Journal of Chemistry, 15(12), 104300.
17. Sardar, A., Khan, S., Hussain, R., Daud, S., Rehman, W., Aziz, T., ... &Alasmari, A. F. (2024). Identification of in vitro α-glucosidase and urease inhibitory effect, and in silico studies of naproxen-derived 1,3,4-oxadiazole-based Schiff-base derivatives. Journal of Molecular Structure, 1305, 137712.
18. Karati, D., Mahadik, K. R., & Kumar, D. (2022). Pyrazole scaffolds: centrality in anti-inflammatory and antiviral drug design. Medicinal Chemistry, 18(10), 1060-1072.
19. Eliwi, A.G., Abdullah, A.M., Abdulsada, S.H., ... Rajab, I.M., Hussein, Z.A (2019), Synthesis and antibacterial activity of some new derivatives containing thiazole moiety and study of their effects on MAO enzyme activity (In vitro). Indian Journal of Public Health Research and Development, 10(1), pp. 1018–1025.
20. Sarvaiya, B. H., Vaja, P. I., Paghdar, N. A., & Ghelani, S. M. (2024). Medicinal perspective of a promising scaffold—dihydropyrimidinones: A review. Journal of Heterocyclic Chemistry, 61(8), 1325-1348.
21. Ali, K. A., Maity, A., Roy, S. D., Pramanik, S. D., Das, P. P., & Shaharyar, M. A. (2023). Insight into the mechanism of steroidal and non-steroidal anti-inflammatory drugs. In How synthetic drugs work (pp. 61-94). Academic Press.
22. de Souza, M. M., Gini, A. L. R., Moura, J. A., Scarim, C. B., Chin, C. M., & Dos Santos, J. L. (2025). The prodrug approach as a strategy to enhance drug permeability. Pharmaceuticals, 18(3), 297.
23. Narayanan, K. B. (2025). Enzyme-Based Anti-Inflammatory Therapeutics for Inflammatory Diseases. Pharmaceutics, 17(5), 606.
24. Narayanan, K. B. (2025). Enzyme-Based Anti-Inflammatory Therapeutics for Inflammatory Diseases. Pharmaceutics, 17(5), 606.
25. Teixeira, S., Castanheira, E. M., & Carvalho, M. A. (2025). Hydrazides as Powerful Tools in Medicinal Chemistry: Synthesis, Reactivity, and Biological Applications. Molecules, 30(13), 2852.
26. Guan, Q., Xing, S., Wang, L., Zhu, J., Guo, C., Xu, C., ... & Sun, H. (2024). Triazoles in medicinal chemistry: physicochemical properties, bioisosterism, and application. Journal of Medicinal Chemistry, 67(10), 7788-7824.
27. Ajmal, M., Mahato, A. K., Khan, M., Rawat, S., Husain, A., Almalki, E. B., ... & Rashid, M. (2024). Significance of Triazole in medicinal chemistry: advancement in drug design, reward, and biological activity. Chemistry & Biodiversity, 21(7), e202400637.
28. Naeem, N., Mughal, E. U., Sadiq, A., Othman, G. A., & Shakoor, B. (2025). Recent Advances in 1, 2, 4-Triazole-Based Anticancer Agents: Structural Optimization, Mechanisms, and Therapeutic Potential (2022–2025). Archiv der Pharmazie, 358(7), e70059.
29. Rohilla, S., Goyal, G., Berwal, P., & Mathur, N. (2024). A review on indole-triazole molecular hybrids as a leading edge in drug discovery: current landscape and future perspectives. Current topics in medicinal chemistry, 24(18), 1557-1588.
30. Ahmadi, M., Bekeschus, S., Weltmann, K. D., von Woedtke, T., & Wende, K. (2022). Non-steroidal anti-inflammatory drugs: Recent advances in the use of synthetic COX-2 inhibitors. RSC medicinal chemistry, 13(5), 471-496.

31. Ahmadi, M., Bekeschus, S., Weltmann, K. D., von Woedtke, T., & Wende, K. (2022). Non-steroidal anti-inflammatory drugs: Recent advances in the use of synthetic COX-2 inhibitors. RSC medicinal chemistry, 13(5), 471-496.
32. Liu, Y., Yang, C., Zhang, J., Ihsan, A., Ares, I., Martínez, M., ... & Martínez, M. A. (2024). Recent progress in adverse events of carboxylic acid non-steroidal anti-inflammatory drugs (CBA-NSAIDs) and their association with the metabolism: the consequences of mitochondrial dysfunction and oxidative stress, and prevention with natural plant extracts. Expert Opinion on Drug Metabolism & Toxicology, 20(8), 765-785.
33. Thiruchenthooran, V., Sánchez-López, E., &Gliszczyńska, A. (2023). Perspectives of the application of non-steroidal anti-inflammatory drugs in cancer therapy: Attempts to overcome their unfavorable side effects. Cancers, 15(2), 475.
34. Sahoo, M. K., Agrawal, N., Lanjhiyana, S. K., Bharti, S. K., & Jaiswal, M. (2025). Therapeutic Perspective of Prodrugs of Non-Steroidal Anti-Inflammatory Drugs and Antioxidants: An Approach to Reduce Toxicity and Enhance Efficacy. Current Topics in Medicinal Chemistry.
35. Nahra, d. m., mohite, p., &deshmukh, s. (2024). emerging pharmacological applications of N-heterocycles: pyrazole derivatives, imidazole derivatives, and triazole derivatives. Paving the Path to Discoveries and Unlocking the Secrets of N-Heterocycles, 148.
36. Kapoor, K., Kaur, N., Sohal, H. S., Kaur, M., Singh, K., & Kumar, A. (2025). Drugs and Their Mode of Action: A Review on Sulfur-Containing Heterocyclic Compounds. Polycyclic Aromatic Compounds, 45(1), 136-175.
37. Aly, A. A., Hassan, A. A., Mohamed, N. K., Abd El-Aal, A. S., Balboul, B. A., Nayl, A. A., ... & Ramadan, M. (2025). Synthesis, Reactions, and Biological Applications of 1, 2, 4-Triazoles: A Review. Current Organic Chemistry, 29(11), 841-868.
38. Tajdari, M., Peyrovinasab, A., Bayanati, M., Rabbani, M. I. M., Abdolghaffari, A. H., &Zarghi, A. (2024). Dual COX-2/TNF-α Inhibitors as Promising Anti-inflammatory and Cancer Chemopreventive Agents: A Review. Iranian Journal of Pharmaceutical Research: IJPR, 23(1), e151312.
39. Al-Wahaibi, L. H., Abdel-Rahman, M. H., El-Adl, K., Youssif, B. G., Brase, S., & Abdel-Aziz, S. A. (2024). New Diaryl-1, 2, 4-triazolo [3, 4-a] pyrimidine hybrids as selective COX-2/sEH dual inhibitors with potent analgesic/anti-inflammatory and cardioprotective properties. ACS omega, 9(31), 33494-33509.
40. Douaa, M., & Sara, S. (2024). Screening of cytotoxic, antithrombotic, and thrombolytic activities of some products and by-products (Doctoral dissertation, university center of Abdelhafid Boussouf-Mila).
41. Sharma, A., Baraiya, R., Prakash, S., Biswas, A., Chowdhury, B., & Sharma, A. (2025). Anti-Inflammatory Potential of Fish-Derived Bioactive Peptides: Molecular Mechanisms, Delivery Strategies, and Clinical Perspectives. Comprehensive Reviews in Food Science and Food Safety, 24(4), e70234.
42. Rajkumar, M., Presley, S. D., Govindaraj, P., Kirubakaran, D., Farahim, Ali, T., ... & Latha, S. (2025). Synthesis of chitosan/PVA/copper oxide nanocomposite using Anacardium occidentale extract and evaluating its antioxidant, antibacterial, anti-inflammatory, and cytotoxic activities. Scientific Reports, 15(1), 3931.
43. Iriawati, I., Vitasasti, S., Rahmadian, F. N. A., &Barlian, A. (2024). Isolation and characterization of plant-derived exosome-like nanoparticles from Carica papaya L. fruit and their potential as anti-inflammatory agents. PLoS One, 19(7), e0304335.
44. Roman, B. H., Muzykiewicz-Szymańska, A., Florkowska, K., Tkacz, M., Wilk, B., Kucharski, Ł., ... & Nowak, A. (2025). The Use of Plants That Seal Blood Vessels in Preparations Applied Topically to the Skin: A Review. Molecules, 30(9), 1973.
45. Kandel, A., Li, L., Wang, Y., Tuo, W., & Xiao, Z. (2024). Differentiation and Regulation of Bovine Th2 Cells In Vitro. Cells 2024, 13, 738. Kandel, A., Li, L., Wang, Y., Tuo, W., & Xiao, Z. (2024). Differentiation and Regulation of Bovine Th2 Cells In Vitro. Cells 2024, 13, 738.
46. Islam, M. S., Al Ferdous, K., Amin, M. N., Kamruzzaman, M., & Islam, M. A. (2024). Impact of monosodium glutamate on the liver of chick embryo: histology, biochemical properties, and AVBD9 gene expression. Int. J. Agric. Biosci., 13, 76-84.
47. Gurjar, S., Bhat, A. R., Upadhya, R., & Shenoy, R. P. (2025). Extracellular vesicle-mediated approaches for the diagnosis and therapy of MASLD: current advances and future prospects. Lipids in Health and Disease, 24(1), 5.
48. Masserdotti, C. (2023). Canine and Feline Liver Cytology. John Wiley & Sons.
49. Holte, C. F. (2024). Novel insights into the fenestrated scavenger endothelium of the liver sinusoid.